Black-wattle tannin/kraft lignin H3PO4-activated carbon xerogels as excellent and sustainable adsorbents

Nicolas Perciani de Moraes, Flávio Henrique Covolam Boldrin, Tiago Moreira Bastos Campos, Gilmar Patrocínio Thim, Yu Lianqing, Marcos Roberto de Vasconcelos Lanza, Liana Alvares Rodrigues

PII: S0141-8130(22)03027-6

DOI: https://doi.org/10.1016/j.ijbiomac.2022.12.125

Reference: BIOMAC 22906

To appear in: *International Journal of Biological Macromolecules*

Received date: 13 October 2022

Revised date: 9 December 2022

Accepted date: 12 December 2022

Please cite this article as: N.P. de Moraes, F.H.C. Boldrin, T.M.B. Campos, et al., Black-wattle tannin/kraft lignin H3PO4-activated carbon xerogels as excellent and sustainable adsorbents, *International Journal of Biological Macromolecules* (2022), https://doi.org/10.1016/j.ijbiomac.2022.12.125

Black-wattle tannin/kraft lignin H_3PO_4-activated carbon xerogels as excellent and sustainable adsorbents

Nicolas Perciani de Moraes[1], Flávio Henrique Covolam Boldrin[2], Tiago Moreira Bastos Campos[3], Gilmar Patrocínio Thim[3], Yu Lianqing[4], Marcos Roberto de Vasconcelos Lanza[1], Liana Alvares Rodrigues[2,*]

1 - Instituto de Química de São Carlos, Universidade de São Paulo, Av. Trab. São Carlense, 400 - Parque Arnold Schimidt, São Carlos - SP, 13566-590

2- Escola de Engenharia de Lorena-EEL/USP, Estrada Municipal do Campinho S/N, CEP 12602-810, Lorena, São Paulo, Brazil.

3- Instituto Tecnológico de Aeronáutica-ITA/CTA, Praça Mal. Eduardo Gomes 50, CEP 12228-900, São José dos Campos, São Paulo, Brazil

4- School of Materials Science and Engineering, China University of Petroleum, QingDao 266580, China

*Corresponding author. Tel.: 55 1231595319; Fax: 55 1231595000

E-mail address: liana.r@usp.br

Abstract

This work proposed new black-wattle tannin/kraft lignin H_3PO_4-activated carbon xerogels as sustainable and efficient adsorbents. The precursors were chosen based on their eco-friendly and cost-effective nature, aiming to achieve adsorbents with high adsorption capacities. Carbon xerogels were synthesized through polycondensation with formaldehyde and alkaline catalyst in a simple one-pot procedure. Activation was performed using H_3PO_4 in a tubular furnace (500 ºC), under a nitrogen atmosphere. Results show that the inclusion of the kraft lignin led to changes in the morphology of the materials, facilitating the development of their porous structure and increasing specific surface area and pore volume. The best adsorbent (XLT 50%) was synthesized using a 1:1 tannin/kraft lignin mass ratio.

This material presented an adsorption capacity of nearly 1150 mg g^{-1} of methylene blue (pH=5 and T=298K), which was linked to its high specific surface area of 1348 m^2 g^{-1}. The adsorption process followed the pseudo-second-order kinetic model, whereas the adsorption isotherms were best fitted by the Sips model. The XLT 50% presented good reusability properties, maintaining its adsorption capacity for 3 cycles. Finally, the XLT 50% presented good adsorptive properties toward other pollutants (methyl orange, 4-chlorophenol, and hexavalent chromium), indicating its versatility for adsorption processes.

Keywords: *Tannin; Kraft lignin; Activated Carbon.*

1. Introduction

Nowadays, the remediation of contaminated industrial wastewater has become one of the main topics of interest investigated by the global scientific community, as the release of toxic effluents into natural aquatic bodies has a catastrophic potential to harm a huge variety of living organisms, including human beings [1,2]. In this context, the release of dyes into the environment by the textile industry has attracted considerable attention, as nearly 20% of the estimated annual production of dyes (700000 tons) has been reportedly discarded into waterbodies throughout the planet [3,4]. As one of the main dyes applied to industrial processes, methylene blue (MB) is of particular interest due to its harmful properties, such as high color saturation in water (inhibiting the algae photosynthesis process) and elevated toxicity to humans, leading to health issues such as respiratory distress, nausea, diarrhea, and paralysis [5,6].

Consequently, the development of efficient, low-cost, and sustainable water treatment processes is of the utmost importance to tackle the aforementioned issue. Recently, several processes surfaced as potential alternatives to the treatment of contaminated effluents, such as heterogeneous photocatalysis, biological treatment, Fenton-based processes, flocculation, etc [7–11]. Among these, adsorption processes using activated carbons have gained considerable

attention due to their elevated efficiency to remediate a large variety of contaminants in aqueous environments, englobing dyes, pesticides, antibiotics, and heavy metals [12–14]. As for the activated carbons used in such processes, great efforts have been applied by the scientific community in order to synthesize cost-effective and highly efficient adsorbents based on natural biomasses, with a special focus on the overall sustainable nature of these materials [15].

With that in mind, the application of industrial carbonaceous byproducts has taken center stage in the development of new adsorbents. As an example, condensed tannins, which are commonly extracted from tree barks, can be considered a particularly suitable precursor for carbonaceous adsorbents [16]. As such, black wattle tannin has been successfully employed as a precursor to carbon xerogels with great adsorption capacities for the remediation of effluents containing phenol and Cr^{3+} [17,18].

Besides condensed tannins, another extremely important carbon precursor obtained as a byproduct in industrial processes can be found in the form of kraft lignin. This material is derived from the Kraft process of cellulose pulping, accounting for approximately 85% of the global lignin production [19]. It is estimated that the paper industry produces more than sixty thousand metric tons of kraft lignin per year, of which only 2% is further commercialized [5]. Recently, the application of kraft lignin was reported in the most diverse fields by related literature, such as biosensors, capacitors, construction materials, controlled release of drugs, tissue engineering, and cosmetics [20–23]. Regarding the adsorption process, lignin is currently applied in the most diverse forms, such as modified lignin, with the inclusion of oxygen, nitrogen, and sulfur-based functional groups, lignin composites, such as SiO_2-lignin and TiO_2-lignin, and various types of adsorbents based on activation processes [1,24]. Considering the tannin molecule previously described, it has been reported that the inclusion of kraft lignin in tannin-based carbon aerogels can extensively modify their porous structure,

resulting in carbonaceous materials with high specific surface areas and pore volumes [25]. However, the further activation of tannin-kraft lignin carbon gels and their application as potential adsorbent materials has not been reported by the related literature, to the best of our knowledge.

Thus, this work proposes the development of simple, sustainable, and cost-effective activated carbons based on tannin/kraft lignin xerogels, focusing on their use as potential adsorbent materials for the remediation of industrial effluents. Furthermore, the adsorbents proposed were extensively characterized in order to understand the effect of the tannin/kraft lignin mass ratio on the adsorption capacity displayed by each material, aiming to obtain an optimized activated carbon fit for application in highly efficient adsorption processes.

2. Materials and methods

2.1 Synthesis of the tannin/kraft lignin H_3PO_4-activated carbon xerogels

Firstly, 0.4 g of potassium hydroxide (KOH, 85 % w/w) was solubilized in 50 mL of deionized water. After that, pre-defined amounts of tannin (PHENOTAN AP, Tanac S.A.) and kraft lignin (provided by Suzano Papel e Celulose S.A.) were added to the solution and kept under magnetic stirring until the complete dissolution of both carbonaceous precursors. Subsequently, 4 mL of formaldehyde solution (37 % w/w) was added to the system, which was then sealed and stored in an oven set at 85ºC. The polycondensation of the gels was carried out for 4 days in the oven. Subsequently to the polycondensation reaction, the monoliths obtained were ground and sifted through a 200-mesh analytical sieve. The materials were then washed with deionized water until pH = 7 was observed in the filtrate.

For the activation with phosphoric acid, 1 g of the obtained tannin-kraft lignin xerogel was mixed with 4 mL of H_3PO_4 (85% w/w) in a porcelain crucible, which was left in

an oven at 85 ºC for 3 h to promote the impregnation process. After that, the mixture was inserted in a tubular muffle furnace and calcined at 500 ºC for 2 h, with a nitrogen atmosphere (0.5 L min^{-1}) and a heating ramp of 10 ºC min^{-1}. The materials obtained were once again washed with deionized water and sieved through a 325 mesh analytical sieve. The activated carbons obtained were named XLT w%, where w% represents the mass percentage of kraft lignin used in the synthesis. Table 1 displays the amounts of tannin and kraft lignin used for each synthesis.

Table 1. Amounts of tannin and kraft lignin used in the preparation of the XLT w%

Material	**Tannin (g)**	**Kraft lignin (g)**
XLT 0%	4	0
XLT 25%	3	1
XLT 50%	2	2
XLT 75%	1	3

2.2 Characterization

The nitrogen isotherms of the samples were recorded using a V-Sorb 2800 device (Gold APP). Initially, the samples were thermally treated for two hours under vacuum at 120 °C. The Brunauer-Emmett-Teller (BET) technique was used to calculate the materials' specific surface areas, whereas the total pore volume was determined at a relative pressure of 0.99. The non-local density functional theory (nLDFT) was used to determine the size distribution of the pores, while the T-plot method was used to define the micropore parameters using the Harkins-Jura model.

A PANalytical X'Pert PRO MPD 3060 diffractometer was employed to obtain the

diffractograms of the XLT w% samples, using a copper X-ray radiation source (CuKα). The following settings were used to run the equipment: 30 mA of current, a voltage of 40 kV, and a step of 0.02 º s^{-1}. A TESCAN MIRA 3 scanning electron microscope with a field emission gun (FEG-SEM), operating in the secondary electron detection mode, was used to examine the morphology of the XLT w%. A Perkin Elmer spectrometer (Frontier model) equipped with a UATR sensor (range: 4000 to 400 cm^{-1}, 16 scans per sample) was used to perform the FT-IR spectroscopy analysis of the XLT w%.

The approach outlined by Wang et al. was used to estimate the point of zero charge (PZC) of the XLT w% [26]. Amber glass bottles were filled with 25 mL of potassium nitrate solution (0.1 mol L^{-1}). By the addition of 0.1 mol L^{-1} NaOH and HCl solutions, the pH of the solution was set in values ranging from 2.5 to 11. To each bottle, 0.05 g of XLT w% was added. The flasks were linearly stirred and shaken for 24 hours in a Dubnoff thermostatic bath.

2.3 Adsorption evaluation

For the adsorption studies, the experiments were conducted in a jacketed beaker maintained at room temperature. 0.02 g of XLT w% was added to the system along with 100 mL of methylene blue (MB) solution. The system was kept under magnetic stirring and samples were collected at predefined times using a syringe and filtered using 0.22 μm nylon filters. The MB concentration in the samples was measured using a Shimadzu UV-2600 UV-Visible spectrophotometer at the wavelength of 673 nm [27].

The effect of pH on the adsorption process was studied using MB solutions (250 mg L^{-1}) with different values of pH. The pH of the system was evaluated in the range between 2 and 11, using 0.1 mol L^{-1} NaOH or HCl solutions to set the pH values. 0.02 g of XLT 50%

was added to the system, and the procedure was carried out as described in the last paragraph.

The effect of the MB concentration on the adsorption process was investigated to determine the adsorption isotherms of MB by the XLT 50%. To that intention, 0.02 g of XLT 50% was added to a jacketed beaker containing 100 mL of MB solution (pH = 5) with concentrations between 125 and 300 mg L^{-1}. This procedure was performed at temperatures ranging from 40 ºC to 60 °C.

The reusability evaluation was performed in the following manner: an XLT 50% sample was subjected to the adsorption process using the optimal conditions determined (pH = 11, C_0 = 250 mg L^{-1}, adsorbent dosage = 0.2 g L^{-1}, V = 0.5 L and T = 25 ºC). After the adsorption equilibrium was reached, the adsorbent was separated and added to 150 mL of ethanol (99% w/w), where it remained under magnetic stirring for 2 h. The adsorbent was then separated from the ethanol solution, washed with deionized water, and dried in an oven at 100 ºC. The dried adsorbent sample was then subjected to another adsorption cycle. The process was repeated for 5 cycles, as described above [28].

The adsorption evaluation for methyl orange (MO), 4-chlorophenol (4CP), and hexavalent chromium (Cr^{6+}) was carried out using the same methodology proposed previously for methylene blue. The methyl orange was detected at the wavelength of 464 nm, whereas the 4-chlorophenol was detected at 224 nm [27,29]. The concentration of Cr^{6+} was calculated by the diphenyl carbazide methodology, using the wavelength of 540 nm [30].

3. Results and discussion

3.1 Characterization

Figure 1 shows the XLT 50% carbon xerogel after the gelation process and before

activation by phosphoric acid.

Figure 1. XLT 50% after the gelation process and before activation by phosphoric acid

As Figure 1 shows, the resulting tannin-kraft lignin xerogel is obtained as a smooth resin-like monolith with dark-brown color. This behavior is characteristic of tannin/formaldehyde-based xerogels produced through alkaline route, indicating high crosslinking between the precursor molecules used in the synthesis [31]. It is also valid to point out that all materials produced displayed the same appearance as the XLT 50%.

Figure 2 shows the X-ray diffractograms of the XLT w% materials synthesized.

Figure 2. X-ray diffractograms obtained for the XLT w% materials

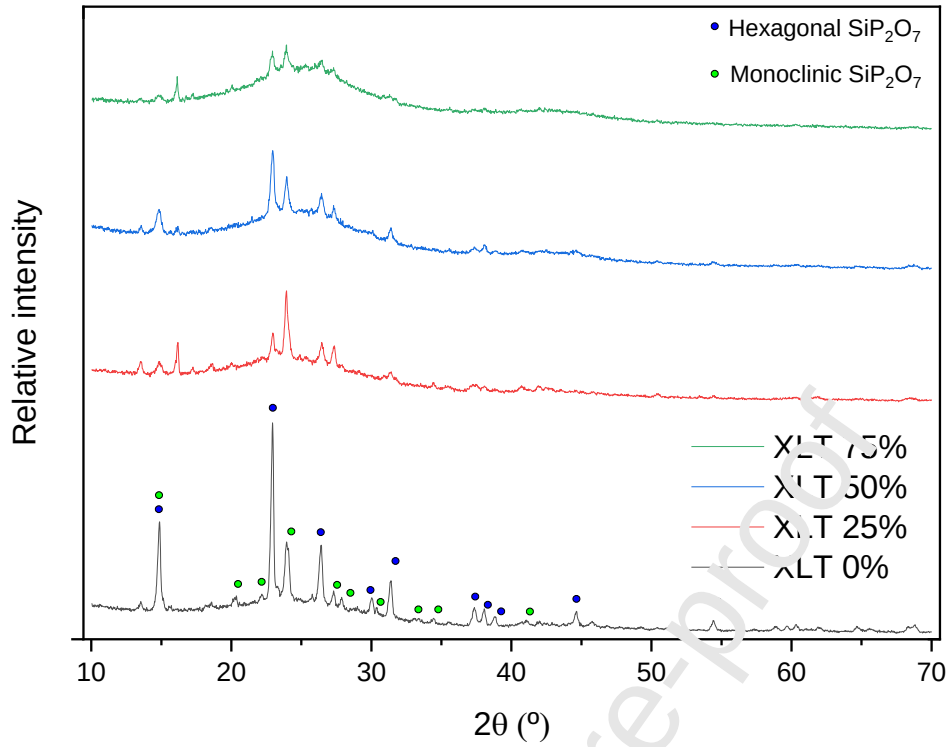

The results obtained show the presence of silicon phosphate (SiP_2O_7) in the structure of the XLT w% materials. This inorganic compound presents itself in the materials in both the hexagonal and monoclinic phases, as indexed in Figure 2. The presence of such silicate is probably linked to the reaction of the silicon present in the tannin with the phosphoric acid used in the activation process, as it is clear that a higher quantity of tannin is intrinsically linked to a higher quantity of SiP_2O_7. Furthermore, it is also possible to notice the presence of a wide halo located in between 20º and 30º, which can be linked to the (002) reflection plane of the turbostratic structure of graphite microcrystallites obtained in the carbonaceous phase [32,33].

Figure 3 shows the infrared spectrum of the XLT w% samples.

Figure 3. Infrared spectrum of the XLT w% materials.

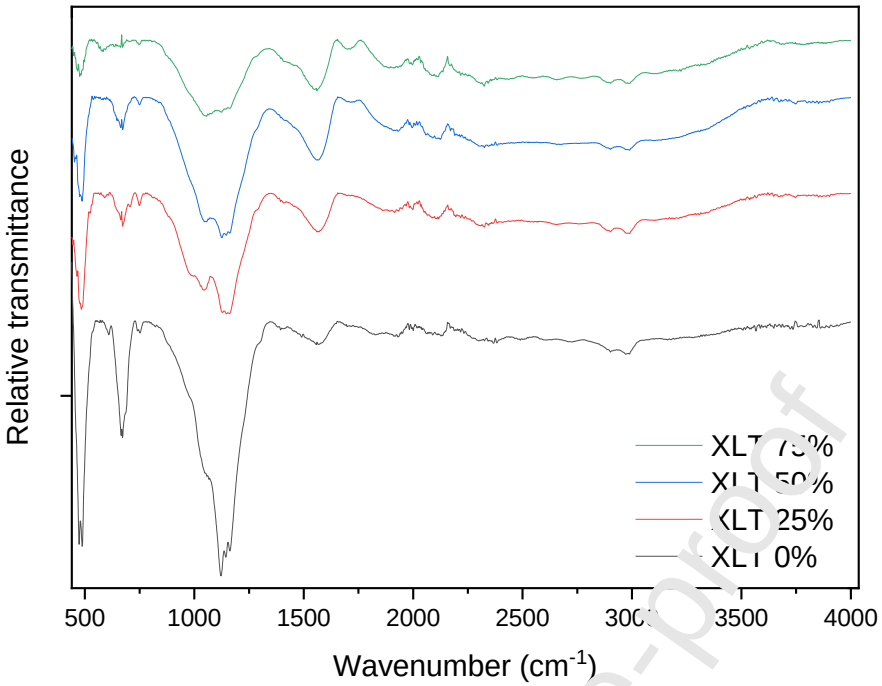

The peaks observed in the spectra of the XLT w% can be identified in the following manner: Si-O-Si bondings (496 and 1158 cm^{-1}), O-P-O bondings (660 cm^{-1}), C=C of skeletal aromatic rings (1560 cm^{-1}), P-C bonding of phosphate functional groups (760 cm^{-1}), P-O groups and C-O bondings from alcoholic groups (1040 cm^{-1}), and C-H from methylene groups (2950 and 3000 cm^{-1}) [24–37]. It is noticeable that the IR results agree with the XRD profiles regarding the presence of the silicon phosphate component, as an increase in the kraft lignin content clearly leads to a reduction of the bands related to the Si-O-Si bondings. Furthermore, the band related to the C=C groups from aromatic rings increases with the addition of kraft lignin to the materials, which is coherent with the complex polymeric structure of this carbonaceous precursor while also evidencing its inclusion into the xerogel's structure.

Figure 4 shows the scanning electron micrographs obtained for the XLT 50% at different magnifications, while Figure 5 shows the micrographs obtained for all XLT w%, at 100000x magnification.

Figure 4. Micrographs obtained for the XLT 50%, at different magnifications: A) 10000x; B) 50000x; C) 200000x and D) 500000x

A) B)

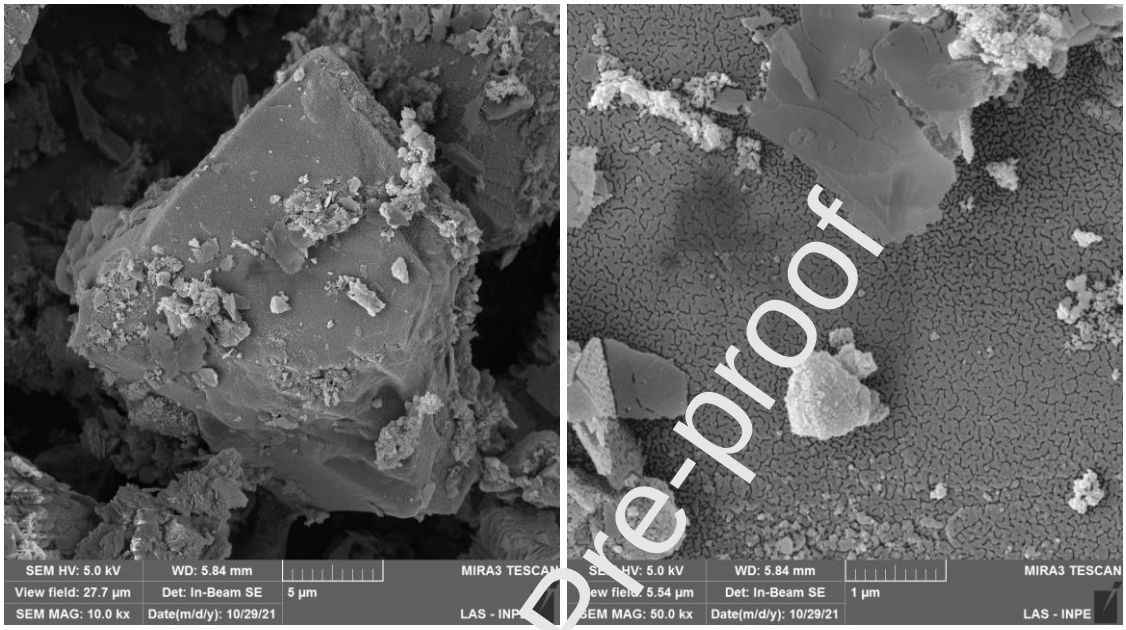

C) D)

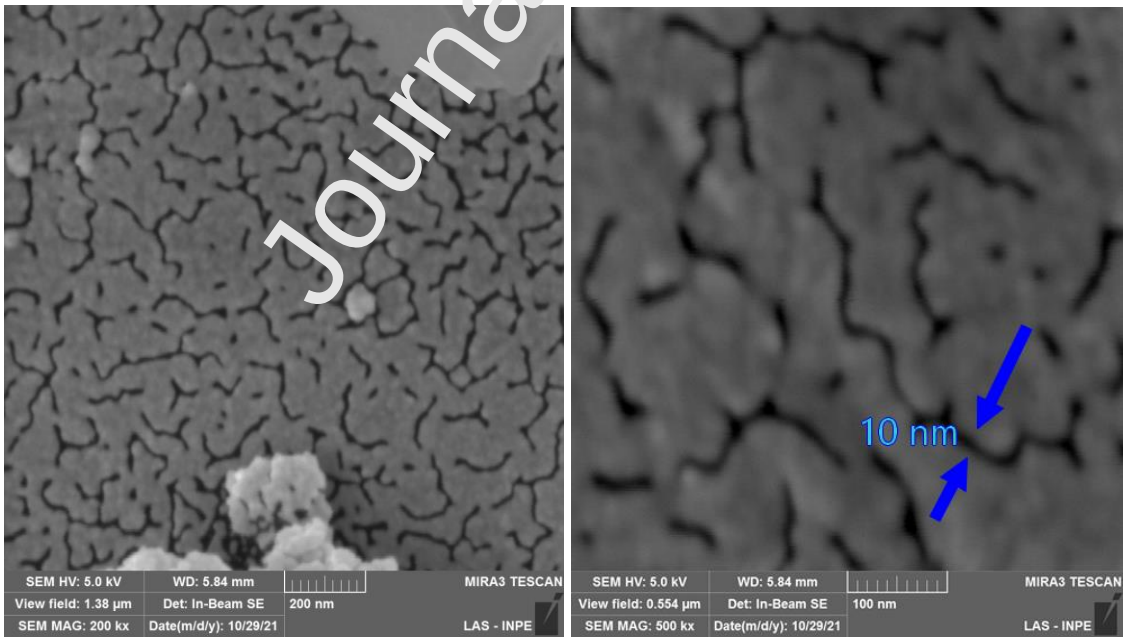

Figure 5. Micrographs obtained for the XLT w%, at 100000x magnification: A) XLT 0%; B) XLT 25%; C) XLT 50% and D) XLT 75%

A) B)

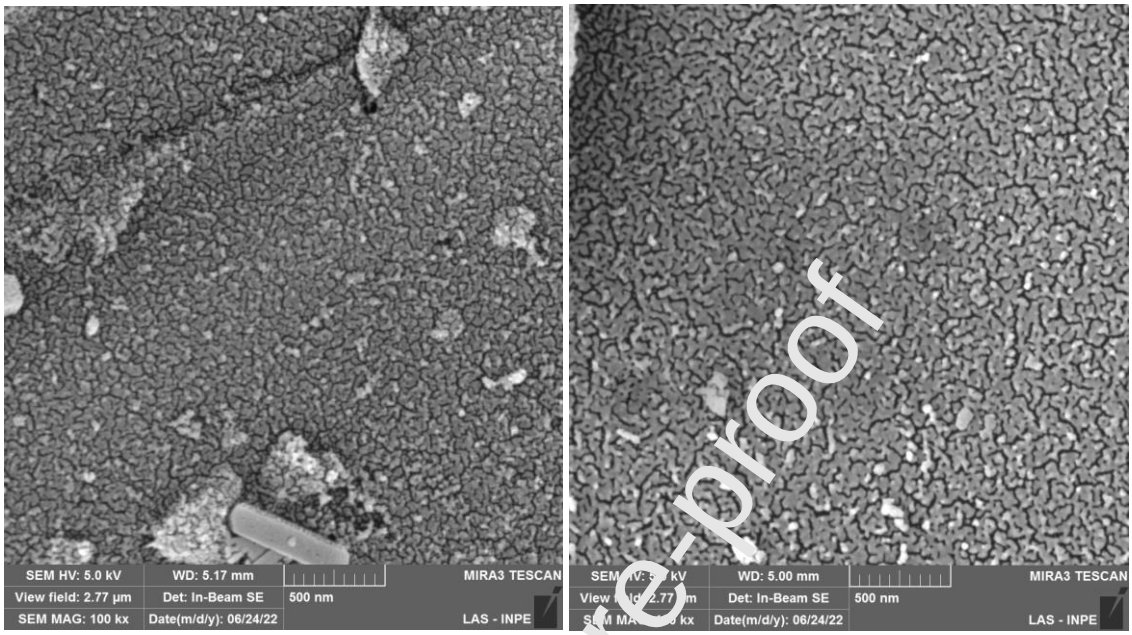

C) D)

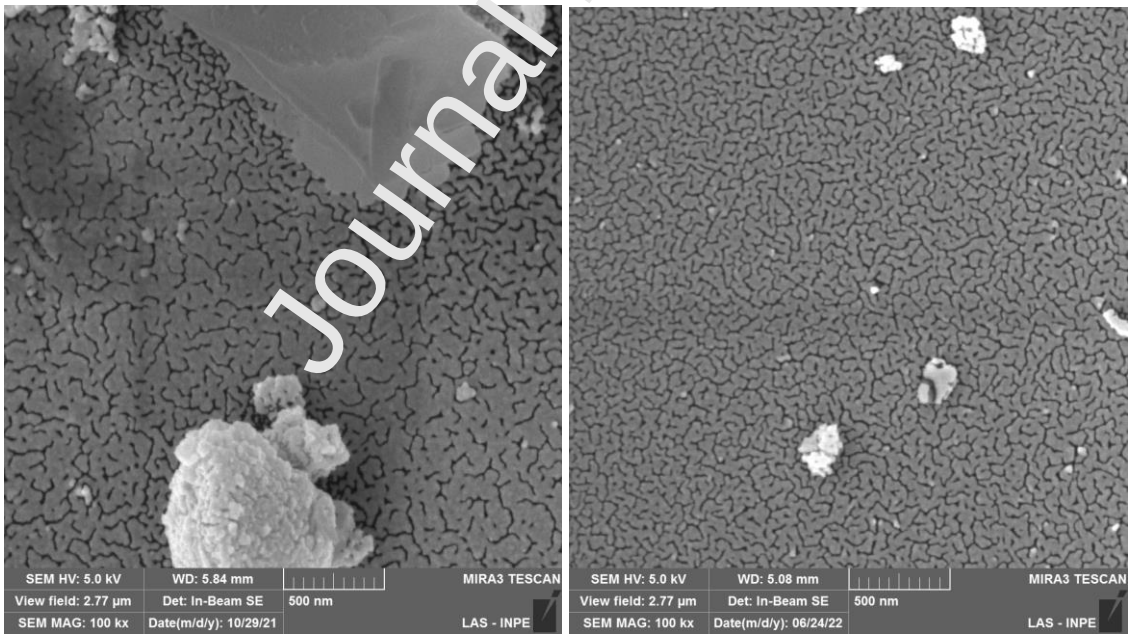

Firstly, Figure 4 shows that the XLT 50% is composed of large polyhedral particles with a large quantity of slit-shaped superficial pores. The pore thickness observed is of

approximately 10 nm, with variable lengths. As for the rest of the materials, Figure 5 shows that the inclusion of the kraft lignin into the xerogel structure led to the creation of deeper more defined pores on the surface of the XLT w%. It is also possible to notice that the XLT 75% presented a more compact porous structure with narrower pores.

Figure 6 and Table 2 display the nitrogen adsorption-desorption isotherms obtained for the XLT w% materials, along with the pore size distribution and the morphological parameters obtained employing the methodologies described in Section 2.2.

Figure 6. A) Nitrogen adsorption-desorption isotherms for the XLT w%; B) Meso and macropore size distribution for the XLT w%; C) Micropore distribution for the XLT w%

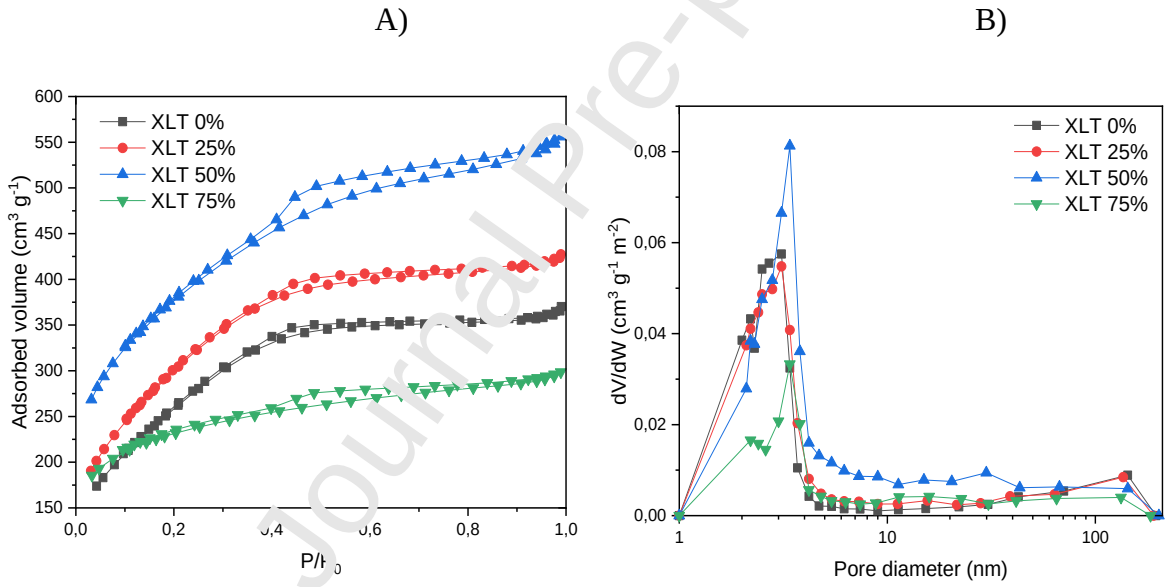

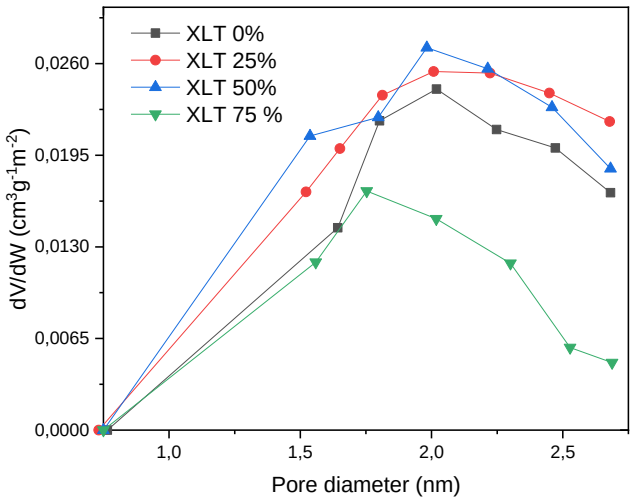

C)

Table 2. Morphological parameters obtained for the XLT w%

Material	Specific surface area (SSA, $m^2 g^{-1}$)	Micropore area ($m^2 g^{-1}$)	Pore volume (PV, $cm^3 g^{-1}$)	Micropore volume ($cm^3 g^{-1}$)
XLT 0%	960.16	105.10	0.5725	0.0183
XLT 25%	1115.48	194.64	0.6610	0.0620
XLT 50%	1348.76	329.13	0.8600	0.1329
XLT 75%	798.75	461.78	0.4618	0.2082

The isotherms of all the XLT w% can be classified as a mixture between types I-H4 and IV-H4, characteristic of micro-mesoporous materials, where the large adsorbed volume at low pressures is suggestive of the presence of micropores and the characteristic behavior of the isotherms at high pressures indicates the formation of mesopores [38]. The type H4 hysteresis loop indicates the presence of narrow slit-like pores, which is consistent with the porous structure observed in the micrographs of the samples [39]. The mesopore size distribution shows that all of the XLT w% materials have porous structures mainly composed of pores in the region between 2-8 nm, which is once again consistent with the micrographs

obtained for the materials. It is also noticeable that the addition of kraft lignin to the xerogels provoked a continuous reduction in the number of macropores with diameters between 100-200 nm. As for the micropore region, the XLT 0%, 25%, and 50% have a main micropore diameter of approximately 2.1 nm, whereas the XLT 75% has a main micropore size of 1.7 nm. Considering the length of the methylene blue molecule which will be used in the adsorption experiments (1.447 nm), the reduction of micropore size in the XLT 75%, coupled with the decrease of available mesopores, will probably cause a negative effect on the adsorption properties of this material [40].

As for the specific surface area of the materials, a continuous enlargement of the micropore network was observed for materials with higher kraft lignin contents. Overall, the specific surface area and pore volume of the materials increased along with the lignin content, except for the material XLT 75%, which displayed the lowest values of SSA and PV among the adsorbents produced. Thus, it is evidenced that the 1:1 mass proportion between tannin and kraft lignin was optimal to increase the SSA and PV of the activated carbon xerogel developed in this work.

3.2 Evaluation of adsorptive properties using the methylene blue cationic dye

Figure 7A shows the effect of contact time for the adsorption of methylene blue using the activated carbons prepared, whereas Figure 7B shows the correlation between the specific surface area of the materials and their maximum adsorption capacity (obtained after using the pseudo-second-order kinetic model described in Equation 2).

Figure 7. A) Adsorption of methylene blue (MB) by the XLT w% materials (V = 100 mL, adsorbent loading = 0.02 g, MB concentration = 250 mg L^{-1}); B) Correlation between the specific surface area of the materials and their maximum adsorption capacity

A) B)

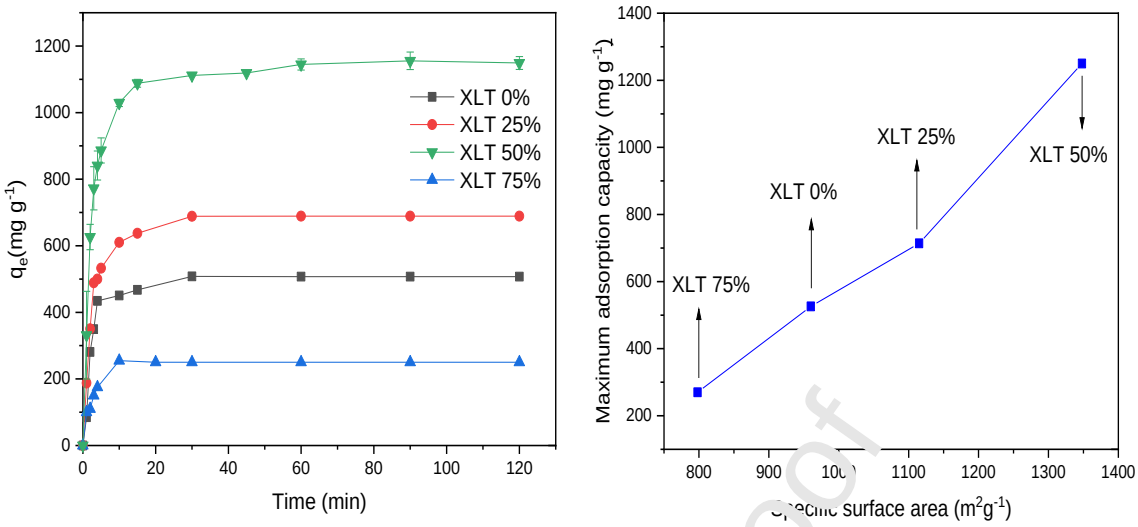

The results obtained show that the XLT 50% achieved the highest adsorption capacity among the materials evaluated, with an equilibrium adsorption capacity of approximately 1150 mg g^{-1} after 60 min. It can be seen from the results displayed in Figure 7B that the maximum adsorption capacities of the activated carbon xerogels are intrinsically linked to their specific surface area, as a nearly linear relation can be derived between these two variables. This result is expected, after all, a higher surface area will provide a greater number of active sites for the adsorption process to take place. Thus, it is highlighted that the inclusion of the kraft lignin in the tannin/formaldehyde xerogel resulted in a superior carbon-based adsorbent for the decontamination of the MB effluent studied in this work.

As for the kinetic evaluation of the adsorption process, the commonly used models are the pseudo-first-order model (Equation 1), the pseudo-second-order model (Equation 2), and the intraparticle diffusion model (Equation 3).

$$\log(q_e - q_t) = \log q_e - \frac{k_1 t}{2.303} \qquad (1)$$

where *qt* and *qe* are the adsorbed amount of MB at a given time (t) and at equilibrium, respectively, and k_1 is the rate constant of the pseudo-first-order adsorption model.

$$\frac{t}{q_t} = \frac{1}{k_2 q_e^2} + \frac{t}{q_e} \quad (2)$$

where k_1 is the rate constant of the pseudo-second-order adsorption model.

$$q_t = k_i t^{0,5} + c_b \quad (3)$$

where k_i is the kinetic constant and c_b is the thickness of the boundary layer of the diffusion process.

Table 3 summarizes the results obtained using the pseudo-first-order and pseudo-second-order kinetic models.

Table 3. Kinetic parameters for the methylene blue adsorption process

Material	**Pseudo-first order**			**Pseudo-second order**		
	k_1 (h^{-1})	q_e(mg g^{-1})	R^2	k_2 (g mg^{-1} h^{-1})	q_e (mg g^{-1})	R^2
XLT 0%	0.161	316.2	0.785	0.00088	526.3	0.995
XLT 25%	0.207	524.8	0.905	0.00067	714.3	0,998
XLT 50%	0.224	870.9	0.939	0.00043	1241.6	0.998
XLT 75%	0.276	229.1	0.960	0.00183	270.3	0.995

Table 3 shows that the pseudo-second-order model better describes the adsorption process studied, as the values of R^2 are closer to 1 and the q_e values are closer to the experimental values obtained. Thus, it is indicated that the rate-limiting step of the MB adsorption onto the XLT w% is the chemical sorption (chemisorption) step.

As for the intraparticle diffusion model, Figure 8 and Table 4 show the results obtained.

Figure 8. Intraparticle diffusion model applied for the XTF w% materials

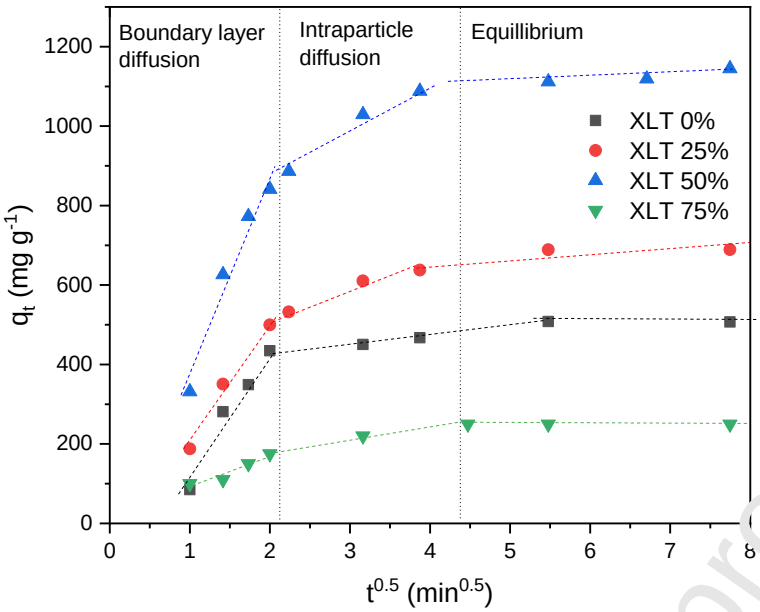

Table 4. Intraparticle diffusion model parameters obtained from the XLT w%

Material	k_1 **(mg g^{-1} min$^{1/2}$)**	**R^2**	k_2 **(mg g^{-1} min$^{1/2}$)**	**R^2**
XLT 0%	290.54	0.98	37.22	0.98
XLT 25%	278.45	0,98	92	0.99
XLT 50%	607.96	0.99	159.6	0.99
XLT 75%	73.6	0.99	45.7	0.98

Figure 8 shows hat, for all materials, the adsorption mechanism described by the intraparticle diffusion model can be separated into three different steps. The first one, which occurs at the initial stages of the adsorption process, can be identified as the boundary-layer diffusion step and is related to the external mass transfer of MB to the surfaces of the XLT w%, leading to adsorption on the external surfaces of the adsorbents. The second step, which was the rate-limiting step for all materials ($k_2 < k_1$), relates to the intraparticle diffusion of the MB onto the active adsorption sites present within the XLT w% particles. Finally, the third step corresponds to the adsorption equilibrium of MB, where all of the active adsorption sites

available have been saturated [41,42].

Figure 9 shows the results of the pH influence on the adsorption capacity obtained by the XLT 50% adsorbent.

Figure 9. Influence of pH on the adsorption capacity of the XLT 50% adsorbent

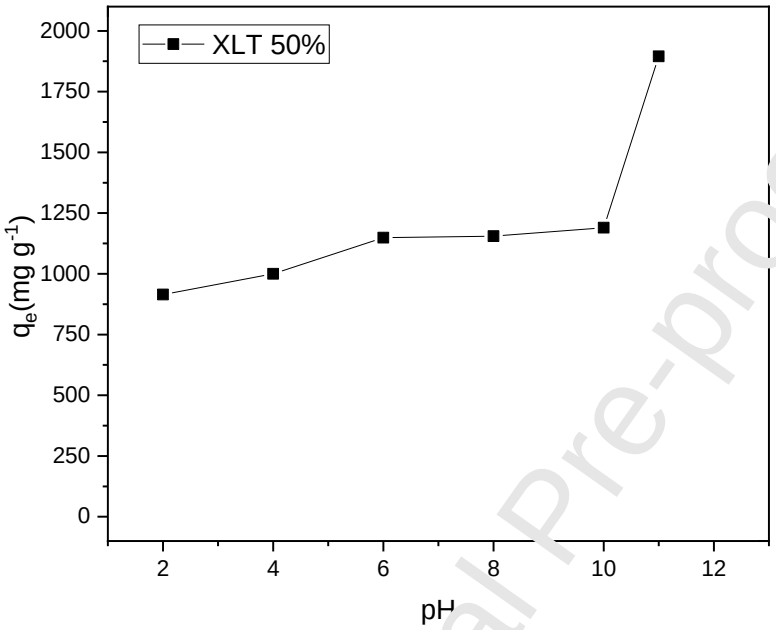

To evaluate the results obtained in Figure 9, it is first necessary to define that point of zero charge value for all the XLT w% was close to pH = 3. Thus, for values of pH > 3, the external surfaces of the adsorbents will be negatively charged. Considering that the MB is a cationic dye, the results obtained are easily explained by the electrostatic interaction between adsorbent and adsorbate. For lower pH values, the surface of the XLT 50% presents a lower negative charge density, which results in a lesser adsorption capacity. As the pH value increases, especially for pH = 11, the surface of the adsorbent becomes more and more negatively charged, boosting the electrostatic attraction taking place between the XLT 50% and the MB molecule and, consequently, increasing the adsorption capacity of the adsorbent [43].

The adsorption isotherms obtained for the XLT 50% at different temperatures

(313,15K, 323,15K, and 333,15K) are displayed in Figure 10. These isotherms were fitted using the following isotherm models: Langmuir (Equation 4), Freundlich (Equation 5), Sips (Equation 6), and Redlich-Peterson (Equation 7) [44–47]. The parameters obtained are displayed in Table 5.

$$\frac{C_e}{q_e} = \frac{1}{q_{max} k_L} + \frac{C_e}{q_{max}} \quad (4)$$

where q_{max} is the maximum amount of MB that may be adsorbed by the XLT 50% (mg g^{-1}), q_e is the adsorption capacity of MB at the equilibrium (mg g^{-1}), *Ce* is the concentration of MB at the adsorption equilibrium (mg L^{-1}) and k_L is the Langmuir adsorption constant (L mg^{-1}).

$$q_e = k_F C_e^{\frac{1}{n}} \quad (5)$$

where k_F (L mg^{-1}) and 1/*n* are the Freundlich isotherm constants.

$$q_e = \frac{q_{max} k_S C_e^n}{1 + k_S C_e^n} \quad (6)$$

where *n* is the Sips model exponent, k_s is the Sips equilibrium constant (L mg^{-1}) and q_{max} is the maximum adsorption capacity.

$$q_e = \frac{k_R C_e}{1 + \alpha C_e^{\beta}} \quad (7)$$

where k_R (L g^{-1}) and α (L mg^{-1}) are the Redlich-Peterson constants and β is the Redlich-Peterson exponential factor.

Figure 10. Adsorption isotherms obtained for the XLT 50% adsorbent, at different temperatures

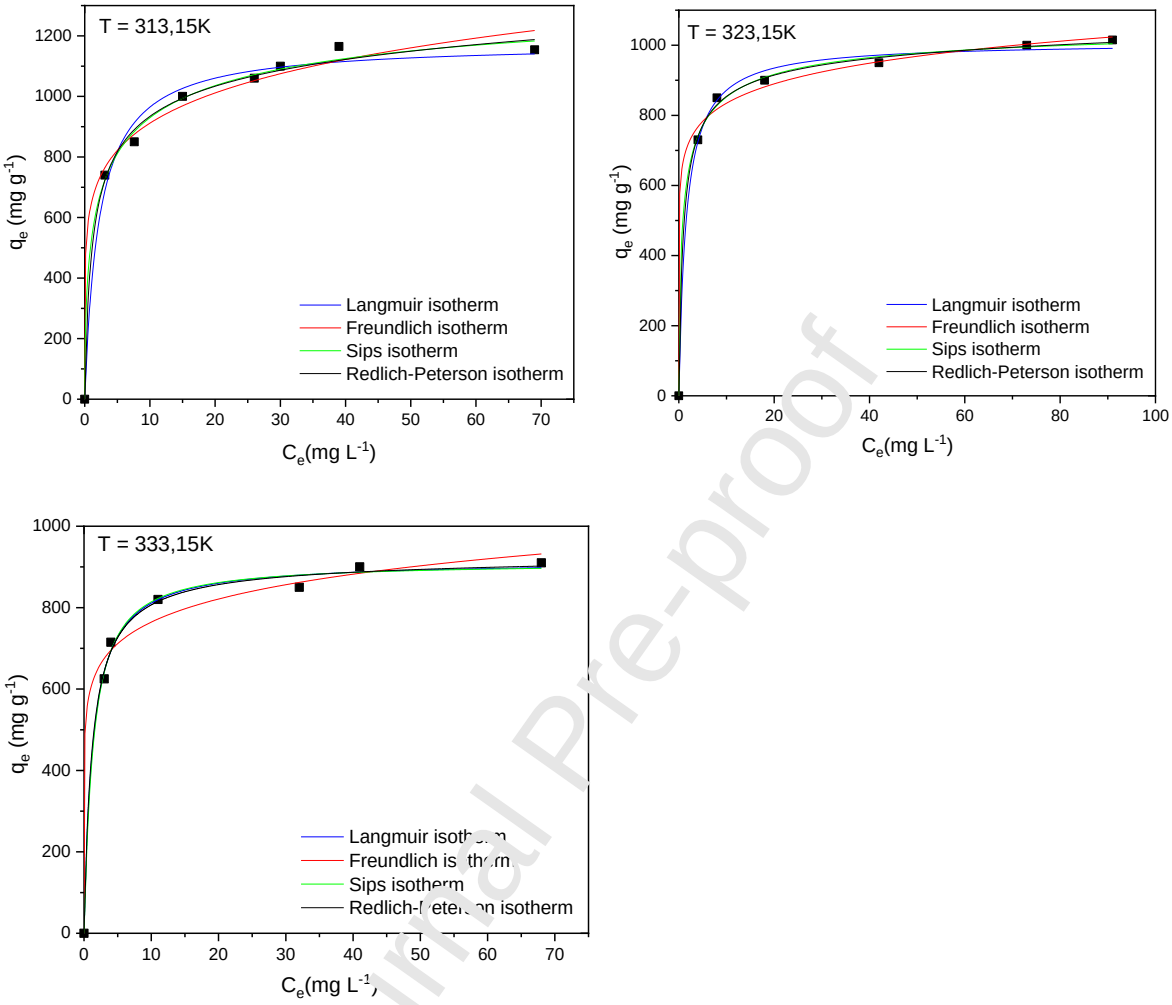

Table 5. Parameters obtained using the proposed isotherm models

Material	**Temperature (K)**	**Langmuir isotherm**			**Freundlich isotherm**		
		q_{max} (mg g^{-1})	k_L (L mg^{-1})	R^2	k_F (L mg^{-1})	n	R^2
XLT 50%	313,15	1176.7	0.45	0.990	645.5	0.15	0.984
	323,15	1008.1	0.64	0.996	674.6	0.09	0.985
	333,15	915.1	0.72	0.996	602.6	0.1	0.98

								8

Material	Temperature (K)	Sips isotherm				Redlich-Peterson isotherm		
		q_{max} (mg g^{-1})	k_S (L mg^{-1})	n	R^2	k_R (L g^{-1})	α (L mg^{-1})	β	R^2
XLT 50%	313,15	1304	0.59	0.52	0.995	1061	1.26	0.91	0.994
	323,15	1072	0.96	0.60	0.998	1070	1.27	0.95	0.998
	333,15	910	0.74	1.05	0.997	775	0.88	0.99	0.995

From the isotherms obtained in Figure 10, it is observed that a correlation between temperature and adsorption capacity exists for the XLT 50%, where an increase in temperature results in a decrease of the observed q_e. As for the isotherm model best suited to describe the adsorption process, the Sips isotherm model achieved the best results, with higher values of R^2 for all isotherms. This model, which is a combination of Langmuir and Freundlich equations, is used to describe the monolayer adsorption process and solve the limitations of the Freundlich model, where the adsorbed amount increases continuously with concentration. Thus, the Sips isotherm model is comparable to the Freundlich model but it has an upper limit when high concentrations are used, converging to the behavior exhibited by the Langmuir isotherm [17,48].

Regarding the thermodynamic parameters of the adsorption process, Gibb's free energy can be defined employing the Van't Hoff equation (Equation 8):

$$\Delta G = -RTlnK_e \quad (8)$$

where ΔG is the Gibbs free energy change, R corresponds to the universal gas constant, T is the adsorption process temperature (K) and K_e is a constant derived from the multiplication of the Langmuir parameters q_{max} and k_L.

With the definition of the ΔG, the enthalpy (ΔH) and entropy changes (ΔS) can be defined using Equation 9:

$$\Delta G = \Delta H - T\Delta S \quad (9)$$

Table 6 gathers the thermodynamic data obtained from the adsorption isotherms of the XLT 50%.

Table 6. Thermodynamic parameters obtained for adsorption of MB by the XLT 50%

Adsorbent	**Temperature (K)**	**ΔG (J·mol^{-1})**	**ΔH (kJ·mol^{-1})**	**ΔS (J·mol^{-1}·K^{-1})**
XLT 50%	313,15	-16219,86398	-9.4	82,3
	323,15	-17272,66712		
	333,15	-17965,76618		

Table 6 shows that the adsorption process studied has an exothermic nature, with a ΔH of -9.4 kJ·mol^{-1}, agreeing with the decreased adsorption capacity at higher temperatures. Furthermore, all values of ΔG obtained were negative, indicating that the MB adsorption process onto the XLT 50% is spontaneous [49].

Figure 11 shows the results obtained for the regeneration and reuse of the XLT 50% in multiple cycles of MB adsorption.

Figure 11. A) Adsorption and desorption of methylene blue after each cycle, using ethanol as a desorbent agent; B) Adsorption capacity of MB after each cycle (pH = 11, C_0 = 250 mg L^{-1},

adsorbent loading = 0.1 g, V = 0.5L)

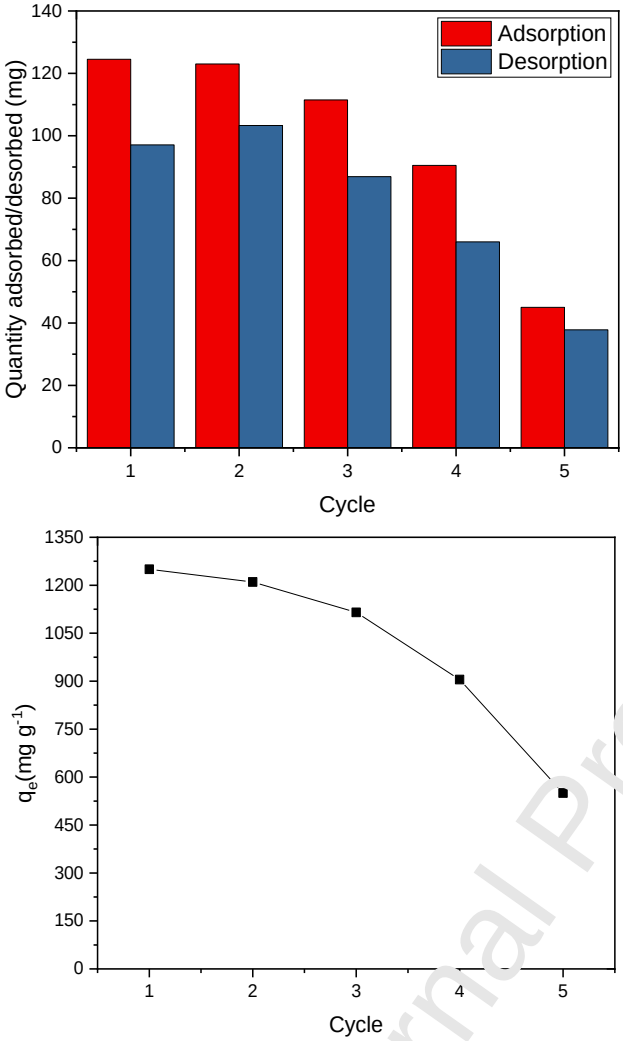

As Figure 11A shows, the use of ethanol as a desorbent for methylene blue was an efficient strategy, especially in the first three cycles, as a desorption percentage of approximately 80% was obtained after each adsorption cycle. However, after cycle number three, the remaining MB present on the surface of the XLT 50% led to a reduction in the adsorption capacity of the material due to the saturation of the available active adsorption sites, as Figure 5B demonstrates. Therefore, the XLT 50% can be reused up to three times without a major efficiency loss.

Finally, Table 7 gathers a comprehensive summary of recently developed biomass-based activated carbons applied for MB adsorption, aiming to contextualize the results obtained in the present work.

Table 7. Comparison between the XLT 50% performance against recently reported biomass-based activated carbons (AC)

Adsorbent	**Specific Surface Area (m^2g^{-1})**	**Adsorption Capacity (mg g^{-1})**	**Reference**
XLT 50%	1348.76	1150	This work
Mangosteen AC	681.4	871.5	[50]
Eucommia ulmoides AC	1135.6	540	[51]
Teak wood waste AC	1345.25	567.5	[52]
Rubber seed pericarp AC	1245.7	347.8	[53]
Ashitaba biomass AC	1505.4	333.5	[54]
Corn fibers AC	820	330.5	[55]
Lignin AC	3382.32	1119.18	[56]
Black liquor AC	1099	307.2	[57]
Kraft lignin AC	1055	220	[58]
Coconut shells AC	935.46	156.2	[59]

As Table 7 shows, the XLT 50% adsorbent developed in this work displayed excellent adsorptive properties when compared to biomass-based materials recently reported in the literature. Thus, it is clear that the adsorbent obtained here is a promising material for application in industrial adsorption processes.

3.3 Evaluation of adsorptive properties using various pollutants

Aiming to further study the versatility of the XLT 50% adsorbent developed in this work, adsorption studies were conducted with various pollutants: methyl orange (an anionic dye), 4-chlorophenol (a pesticide with pKa = 9), and hexavalent chromium (a heavy metal

toxic cation) [60–62]. All the adsorption tests for these molecules were performed at pH = 5 and ambient temperature. Figure 12 and Table 8 show the results obtained for the aforementioned tests.

Figure 12. Adsorption isotherms for: A) Methyl orange; B) 4-chlorophenol; C) Hexavalent chromium

A)

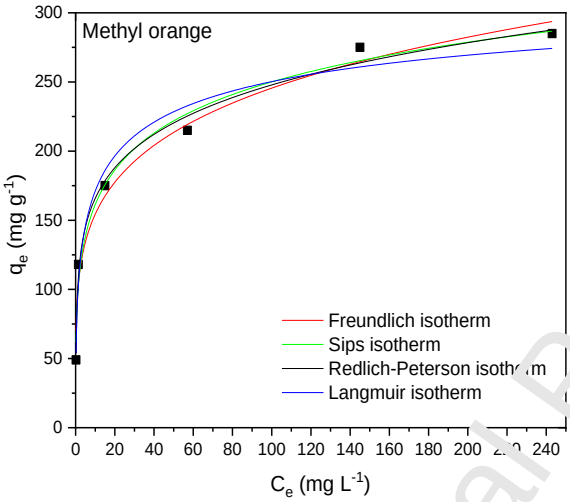

B)

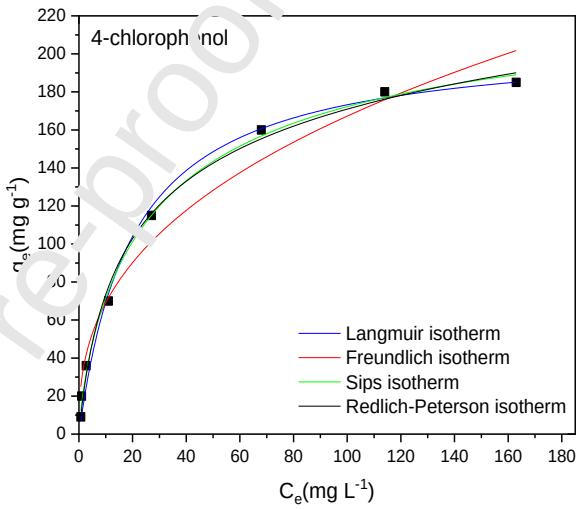

C)

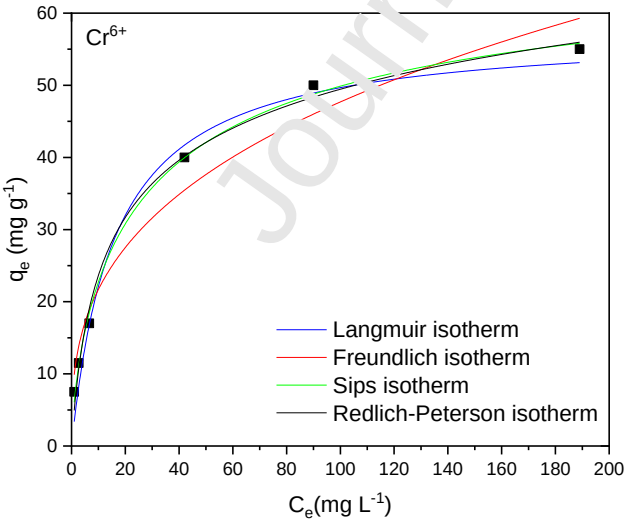

Table 8. Parameters obtained using the proposed isotherm models

Material	**Pollutant**	**Langmuir isotherm**			**Freundlich isotherm**		
		q_{max} (mg g^{-1})	k_L (L mg^{-1})	R^2	k_F (L mg^{-1})	n	R^2
XLT 50%	Methyl orange	346	0.36	0.973	97	0.2	0.972
	4-chlorophenol	208	0.05	0.991	28.6	0.38	0.965
	Cr^{6+}	57.6	0.06	0.967	9.87	0.34	0.959

Material	Pollutant	Sips isotherm				Redlich-Peterson isotherm			
		q_{max} (mg g^{-1})	k_S (L mg^{-1})	n	R^2	k_R (L g^{-1})	α (L mg^{-1})	β	R^2
XLT 50%	Methyl orange	542	0.21	0.30	0.989	674	5.8	0.83	0.985
	4-chlorophenol	239.6	0.07	0.77	0.996	15.5	0.15	0.86	0.993
	Cr^{6+}	70.8	0.09	0.70	0.994	5.95	0.21	0.86	0.988

As the results show, the XLT 50% is able to adsorb all the pollutants evaluated, to different extents of adsorption capacity, independently of the nature of the adsorbate. As previously, the Sips isotherm model presented the best fit for the results obtained and the maximum adsorption capacities found were 542 mg g^{-1} for the MO, 239.6 mg g^{-1} for the 4CP, and 70.8 mg g^{-1} for Cr^{6+}. To better contextualize these results, Table 9 shows a comparison between the results obtained in this work and those previously reported in the related literature.

Table 9. Comparison between the results obtained in this work and the ones reported in the related literature for the adsorption of methyl orange, 4-chlorophenol and hexavalent chromium

Pollutant	**Adsorbent**	**Adsorption Capacity (mg g^{-1})**	**Reference**
Methyl orange	XLT 50%	542	This work
	Coffee grounds AC	658	[63]
	Orange and lemon peel AC	33	[64]
	Vitis vinifera L. AC	79.7	[65]
	Waste-cellulose AC	337.8	[66]
	Pomelo peel AC	163.1	[67]
4-chlorophenol	XLT 50%	239.6	This work
	Rattan sawdust AC	188	[68]
	Sewage sludge AC	174	[69]
	Milk vetch AC	87	[70]
	Wheat straw biochar	111	[71]
	Coconut shell AC	85.8	[72]
Hexavalent chromium	XLT 50%	70.8	This work
	Apple peels AC	36	[73]
	Peanut shell AC	16.3	[74]
	Mango kernel AC	7.8	[75]
	Corn stalk AC	89.5	[76]

The data collected in Table 9 show that the material developed in this work presents a good adsorption capacity for the pollutants evaluated in this section, further highlighting its

potential application in a diverse range of industrial adsorption processes.

Conclusion

It is concluded that the tannin/kraft lignin H_3PO_4-activated carbon xerogels, particularly the XLT 50%, are excellent adsorbents for the methylene blue molecule. This result is derived from the inclusion of the kraft lignin to the tannin/formaldehyde xerogel, which promoted a higher development of the porous structure of the XLT 50% while also increasing its specific surface area and pore volume. At regular conditions, the XLT 50% presented an adsorption capacity of approximately 1150 mg g^{-1} (pH = 5 and T = 298K), which is an excellent result when compared to related works in the literature. The MB adsorption kinetics can be described by the pseudo-second-order model, whereas the adsorption isotherms follow the Sips isotherm model. Furthermore, the XLT 50% can be reused up to three times without major loss in its methylene blue adsorption capacity. Finally, the results show that the XLT 50% can be used to perform adsorption processes using a wide range of pollutants, evidencing its suitability for real-world applications.

Acknowledgments

The authors acknowledge the financial support provided by the São Paulo Research Foundation (FAPESP) (Grants Nº 2018/10492-1, Nº 2018/16360-0, Nº 2022/04058-2 and Nº 2017/10118-0). The authors are also grateful to TANAC S.A., which supplied the black wattle tannin, and to Suzano Papel e Celulose S.A., which supplied the kraft lignin.

References

[1] Suhas, P.J.M. Carrott, M.M.L. Ribeiro Carrott, Lignin - from natural adsorbent to activated carbon: A review, Bioresour. Technol. 98 (2007) 2301–2312. https://doi.org/10.1016/j.biortech.2006.08.008.

[2] A.E. Burakov, E. V. Galunin, I. V. Burakova, A.E. Kucherova, S. Agarwal, A.G. Tkachev, V.K. Gupta, Adsorption of heavy metals on conventional and nanostructured

materials for wastewater treatment purposes: A review, Ecotoxicol. Environ. Saf. 148 (2018) 702–712. https://doi.org/10.1016/j.ecoenv.2017.11.034.

[3] X. Wan, Z. Rong, K. Zhu, Y. Wu, Chitosan-based dual network composite hydrogel for efficient adsorption of methylene blue dye, Int. J. Biol. Macromol. 222 (2022) 725–735. https://doi.org/10.1016/j.ijbiomac.2022.09.213.

[4] K. Fan, T. Zhang, S. Xiao, H. He, J. Yang, Z. Qin, Preparation and adsorption performance of functionalization cellulose-based composite aerogel, Int. J. Biol. Macromol. 211 (2022) 1–14. https://doi.org/10.1016/J.IJBIOMAC.2022.05.042.

[5] L.F.B. de Araújo, S.E. Mazzetto, D. Lomonaco, F. Avelino, Unraveling the adsorption mechanism of methylene blue onto selective pH precipitated Kraft lignins: Kinetic, equilibrium and thermodynamic aspects, Int. J. Biol. Macromol. 220 (2022) 1267–1276. https://doi.org/10.1016/J.IJBIOMAC.2022.08.195.

[6] Z. Wu, Q. Liao, P. Chen, D. Zhao, J. Huo, M. An, Y. Li, J. Wu, Z. Xu, B. Sun, M. Huang, Synthesis, characterization, and methylene blue adsorption of multiple-responsive hydrogels loaded with Huangshui polysaccharides, polyvinyl alcohol, and sodium carboxyl methyl cellulose, Int. J. Biol. Macromol. 216 (2022) 157–171. https://doi.org/10.1016/J.IJBIOMAC.2022.06.178.

[7] Z. Wei, J. Liu, W. Shangguan, A review on photocatalysis in antibiotic wastewater: Pollutant degradation and hydrogen production, Chinese J. Catal. 41 (2020) 1440–1450. https://doi.org/10.1016/S1872-2067(19)63448-0.

[8] S. Rahim Pouran, A.R. Abdul Aziz, W.M.A. Wan Daud, Review on the main advances in photo-Fenton oxidation system for recalcitrant wastewaters, J. Ind. Eng. Chem. 21 (2015) 53–69. https://doi.org/10.1016/j.jiec.2014.05.005.

[9] M. Kurian, Advanced oxidation processes and nanomaterials -a review, Clean. Eng. Technol. 2 (2021) 100090. https://doi.org/10.1016/j.clet.2021.100090.

[10] M. Chethana, L.G. Sorokhaibam, V.M. Bhandari, S. Raja, V. V. Ranade, Green Approach to Dye Wastewater Treatment Using Biocoagulants, ACS Sustain. Chem. Eng. 4 (2016) 2495–2507. https://doi.org/10.1021/acssuschemeng.5b01553.

[11] C.L.S. Vilela, J.P. Bassin, R.S. Peixoto, Water contamination by endocrine disruptors: Impacts, microbiological aspects and trends for environmental protection, Environ. Pollut. 235 (2018) 546–559. https://doi.org/10.1016/j.envpol.2017.12.098.

[12] F.M. Mpatani, R. Han, A.A. Aryee, A.N. Kani, Z. Li, L. Qu, Adsorption performance of modified agricultural waste materials for removal of emerging micro-contaminant bisphenol A: A comprehensive review, Sci. Total Environ. 780 (2021) 146629. https://doi.org/10.1016/j.scitotenv.2021.146629.

[13] C. Namasivayam, D. Sangeetha, Recycling of agricultural solid waste, coir pith: Removal of anions, heavy metals, organics and dyes from water by adsorption onto ZnCl2 activated coir pith carbon, J. Hazard. Mater. 135 (2006) 449–452. https://doi.org/10.1016/j.jhazmat.2005.11.066.

[14] N. Li, Q.-S. Liu, T. Zheng, J. F. Jiang, P. Wang, Adsorption isotherm, kinetic and mechanism studies of some substituted phenols on activated carbon fibers, Chem. Eng. J. 157 (2009) 348–356. https://doi.org/10.1016/j.cej.2009.11.013.

[15] G. Jaria, V. Calisto, V.I. Esteves, M. Otero, Overview of relevant economic and environmental aspects of waste-based activated carbons aimed at adsorptive water treatments, J. Clean. Prod. 344 (2022) 130984. https://doi.org/10.1016/J.JCLEPRO.2022.130984.

[16] D.K. Sam, E.K. Sam, A. Durairaj, X. Lv, Z. Zhou, J. Liu, Synthesis of biomass-based carbon aerogels in energy and sustainability, Carbohydr. Res. 491 (2020) 107986. https://doi.org/10.1016/j.carres.2020.107986.

[17] L.A. Rodrigues, T.M.B. Campos, M.O. Alvarez-Mendes, A.D.R. Coutinho, K.K.

Sakane, G.P. Thim, Phenol removal from aqueous solution by carbon xerogel, J. Sol-Gel Sci. Technol. 63 (2012) 202–210. https://doi.org/10.1007/s10971-012-2745-3.

[18] L. Alvares Rodrigues, K. Koibuchi Sakane, E. Alves Nunes Simonetti, G. Patrocínio Thim, Cr total removal in aqueous solution by PHENOTAN AP based tannin gel (TFC), J. Environ. Chem. Eng. (2015). https://doi.org/10.1016/j.jece.2015.04.006.

[19] N.M.A. Al-Lagtah, A.H. Al-Muhtaseb, M.N.M. Ahmad, Y. Salameh, Chemical and physical characteristics of optimal synthesised activated carbons from grass-derived sulfonated lignin versus commercial activated carbons, Microporous Mesoporous Mater. 225 (2016) 504–514. https://doi.org/10.1016/J.MICROMESO.2016.01.043.

[20] A. Beaucamp, M. Muddasar, T. Crawford, M.N. Collins, M. Culebras, Sustainable lignin precursors for tailored porous carbon-based supercapacitor electrodes., Int. J. Biol. Macromol. 221 (2022) 1142–1149. https://doi.org/10.1016/J.IJBIOMAC.2022.09.097.

[21] P. Jędrzejczak, M.N. Collins, T. Jesionowski, Ł. Klapiszewski, The role of lignin and lignin-based materials in sustainable construction – A comprehensive review, Int. J. Biol. Macromol. 187 (2021) 624–650. https://doi.org/10.1016/J.IJBIOMAC.2021.07.125.

[22] M. Culebras, M. Pishnamazi, G.M. Walker, M.N. Collins, Facile Tailoring of Structures for Controlled Release of Paracetamol from Sustainable Lignin Derived Platforms, Mol. 2021, Vol. 26, Page 1593. 26 (2021) 1593. https://doi.org/10.3390/MOLECULES26061593.

[23] M. Stanisz, Klapiszewski, M.N. Collins, T. Jesionowski, Recent progress in biomedical and biotechnological applications of lignin-based spherical nano- and microstructures: a comprehensive review, Mater. Today Chem. 26 (2022) 101198. https://doi.org/10.1016/j.mtchem.2022.101198.

[24] Y. Ge, Z. Li, Application of Lignin and Its Derivatives in Adsorption of Heavy Metal Ions in Water: A Review, ACS Sustain. Chem. Eng. 6 (2018) 7181–7192. https://doi.org/10.1021/ACSSUSCHEMENG.8B01345/ASSET/IMAGES/LARGE/SC-2018-01345F_0006.JPEG.

[25] L.I. Grishechko, G. Amaral-Labat, A. Szczurek, V. Fierro, B.N. Kuznetsov, A. Pizzi, A. Celzard, New tannin-lignin aerogels, Ind. Crops Prod. 41 (2013) 347–355. https://doi.org/10.1016/j.indcrop.2012.04.052.

[26] L. Wang, J. Zhang, A. Wang, Removal of methylene blue from aqueous solution using chitosan-g-poly(acrylic acid)/montmorillonite superadsorbent nanocomposite, Colloids Surfaces A Physicochem. Eng. Asp. 322 (2008) 47–53. https://doi.org/10.1016/j.colsurfa.2008.02.019

[27] N.P. de Moraes, F.A. Torezin, G.V. Jurá Dantas, J.G.M. de Sousa, R.B. Valim, R. da Silva Rocha, R. Landers, M.L.C.P. da Silva, L.A. Rodrigues, TiO2/Nb2O5/carbon xerogel ternary photocatalyst for efficient degradation of 4-chlorophenol under solar light irradiation, Ceram. Int. 46 (2020) 14505–14515. https://doi.org/10.1016/j.ceramint.2020.02.249.

[28] W. Huang, J. Chen, J. Zhang, Adsorption characteristics of methylene blue by biochar prepared using sheep, rabbit and pig manure, Environ. Sci. Pollut. Res. 25 (2018) 29256–29266. https://doi.org/10.1007/s11356-018-2906-1.

[29] S. Zarrin, F. Heshmatpour, Photocatalytic activity of TiO2/Nb2O5/PANI and TiO2/Nb2O5/RGO as new nanocomposites for degradation of organic pollutants, J. Hazard. Mater. 351 (2018) 147–159. https://doi.org/10.1016/j.jhazmat.2018.02.052.

[30] APHA, Standard Methods for the Examination of Water and Wastewater. Federation. Water Environmental American Public Health Association (APHA),Washington, DC, USA., Fed. Washingt. DC. (2017).

[31] N. Rey-Raap, A. Szczurek, V. Fierro, A. Celzard, J.A. Menéndez, A. Arenillas, Advances in tailoring the porosity of tannin-based carbon xerogels, Ind. Crops Prod. 82 (2016) 100–106. https://doi.org/10.1016/j.indcrop.2015.12.001.

[32] H. Hadoun, Z. Sadaoui, N. Souami, D. Sahel, I. Toumert, Characterization of mesoporous carbon prepared from date stems by H 3PO4 chemical activation, Appl. Surf. Sci. 280 (2013) 1–7. https://doi.org/10.1016/j.apsusc.2013.04.054.

[33] J.R.C. Nobre, J.P. Castro, M.L. Bianchi, W. Miguel, P.F. Trugilho, S cientia F orestalis Caracterização do carvão ativado produzido a partir de serragens de maçaranduba Characterization of activated carbon produced from sawdust massaranduba, Sci. For. Sci. 43 (2015) 693–702.

[34] C. Weinberger, T. Heckel, P. Schnippering, M. Schmitz, A. Guo, W. Keil, H.C. Marsmann, C. Schmidt, M. Tiemann, R. Wilhelm, Straightforward immobilization of phosphonic acids and phosphoric acid esters on mesoporous silica and their application in an asymmetric aldol reaction, Nanomaterials. 9 (2019). https://doi.org/10.3390/nano9020249.

[35] N.P. de Moraes, R. da Silva Rocha, A. de Siervo, C.C.A. do Prado, T.C.B. de Paiva, T.M.B. Campos, G.P. Thim, M.R. de Vasconcelos Lanza, L.A. Rodrigues, Resorcinol-based carbon xerogel/ZnO composite for solar-light-induced photodegradation of sulfamerazine, Opt. Mater. (Amst). 128 (2022). https://doi.org/10.1016/j.optmat.2022.112470.

[36] K. Ohwada, Infrared Spectra of Organic Phosphates in the Combination Region of the C–O and P–O Vibrations, Appl. Spectrosc. Vol. 22, Issue 3, Pp. 209-209. 22 (1968) 209–209. https://opg.optica.org/abstract.cfm?uri=as-22-3-209 (accessed September 23, 2022).

[37] W. Jastrzbski, M. Sitarz, M. Rokita, K. Bułat, Infrared spectroscopy of different

phosphates structures, Spectrochim. Acta Part A Mol. Biomol. Spectrosc. 79 (2011) 722–727. https://doi.org/10.1016/J.SAA.2010.08.044.

[38] R. Khatoon, S. Attique, R. Liu, S. Rauf, N. Ali, L. Zhang, Y.J. Zeng, Y. Guo, Y.V. Kaneti, J. Na, H. Tang, H. Chen, Y. Tian, J. Lu, Carbonized waste milk powders as cathodes for stable lithium–sulfur batteries with ultra-large capacity and high initial coulombic efficiency, Green Energy Environ. 7 (2022) 1071–1083. https://doi.org/10.1016/J.GEE.2021.01.007.

[39] R. Bardestani, G.S. Patience, S. Kaliaguine, Experimental methods in chemical engineering: specific surface area and pore size distribution measurements—BET, BJH, and DFT, Can. J. Chem. Eng. 97 (2019) 2781–2791. https://doi.org/10.1002/CJCE.23632.

[40] P. Jia, H. Tan, K. Liu, W. Gao, Removal of methylene blue from aqueous solution by bone char, Appl. Sci. 8 (2018). https://doi.org/10.3390/app8101903.

[41] C.S. Cheng, J. Deng, B. Lei, A. He, X. Zhang, L. Ma, S. Li, C. Zhao, Toward 3D graphene oxide gels based adsorbents for high-efficient water treatment via the promotion of biopolymers, J. Hazard. Mater. 263 (2013) 467–478. https://doi.org/10.1016/j.jhazmat.2013.09.065.

[42] C. Feng, P. Ren, Z. Li, W. Tan, H. Zhang, Y. Jin, F. Ren, Graphene/waste-newspaper cellulose composite aerogels with selective adsorption of organic dyes: Preparation, characterization, and adsorption mechanism, New J. Chem. 44 (2020) 2256–2267. https://doi.org/10.1039/c9nj05346h.

[43] R.K. Ramakrishnan, V.V.T. Padil, S. Wacławek, M. Černík, R.S. Varma, Eco-Friendly and Economic, Adsorptive Removal of Cationic and Anionic Dyes by Bio-Based Karaya Gum—Chitosan Sponge, Polym. 2021, Vol. 13, Page 251. 13 (2021) 251. https://doi.org/10.3390/POLYM13020251.

[44] W.Z. Durrani, A. Nasrullah, A.S. Khan, T.M. Fagieh, E.M. Bakhsh, K. Akhtar, S.B. Khan, I.U. Din, M.A. Khan, A. Bokhari, Adsorption efficiency of date palm based activated carbon-alginate membrane for methylene blue, Chemosphere. 302 (2022) 134793. https://doi.org/10.1016/J.CHEMOSPHERE.2022.134793.

[45] L.A. Rodrigues, M.L.C.P. da Silva, Thermodynamic and kinetic investigations of phosphate adsorption onto hydrous niobium oxide prepared by homogeneous solution method, Desalination. 263 (2010) 29–35. https://doi.org/10.1016/j.desal.2010.06.030.

[46] L.A. de Sousa Ribeiro, G.P. Thim, M.O. Alvarez-Mendez, A. dos Reis Coutinho, N.P. de Moraes, L.A. Rodrigues, Preparation, characterization, and application of low-cost açaí seed-based activated carbon for phenol adsorption, Int. J. Environ. Res. 12 (2018) 755–764. https://doi.org/10.1007/s41742-018-0128-5.

[47] S. Kalam, S.A. Abu-Khamsin, M.S. Kamal, S. Patil, Surfactant Adsorption Isotherms: A Review, ACS Omega. 6 (2021) 32342–32348. https://doi.org/10.1021/acsomega.1c04661.

[48] Saruchi, V. Kumar, Adsorption kinetics and isotherms for the removal of rhodamine B dye and Pb +2 ions from aqueous solutions by a hybrid ion-exchanger, Arab. J. Chem. 12 (2019) 316–329. https://doi.org/10.1016/j.arabjc.2016.11.009.

[49] W. Meng, Z. Ma, J. Shu, B. Li, P. Su, R. Wang, M. Chen, Z. Liu, K. Ai, Efficient adsorption of methylene blue from aqueous solution by hydrothermal chemical modification phosphorus ore flotation tailings, Sep. Purif. Technol. 281 (2022) 119496. https://doi.org/10.1016/J.SEPPUR.2021.119496.

[50] A.H. Jawad, S.E.M. Saber, A.S. Abdulhameed, A. Reghioua, Z.A. ALOthman, L.D. Wilson, Mesoporous activated carbon from mangosteen (Garcinia mangostana) peels by H3PO4 assisted microwave: Optimization, characterization, and adsorption mechanism for methylene blue dye removal, Diam. Relat. Mater. (2022) 109389.

https://doi.org/10.1016/J.DIAMOND.2022.109389.

[51] Q.Q. Zhou, L. Qiu, M.Q. Zhu, Eucommia ulmoides Oliver derived magnetic activated carbon for eliminating methylene blue from dyeing wastewater and its economic efficiency assessment, Ind. Crops Prod. 187 (2022) 115537. https://doi.org/10.1016/J.INDCROP.2022.115537.

[52] M. Firdaus Mohamad Yusop, A. Aziz, M. Azmier Ahmad, Conversion of teak wood waste into microwave-irradiated activated carbon for cationic methylene blue dye removal: Optimization and batch studies, Arab. J. Chem. 15 (2022) 104081. https://doi.org/10.1016/J.ARABJC.2022.104081.

[53] A.H. Jawad, N.N.A. Malek, T. Khadiran, Z.A. ALOthman, Z.M. Yaseen, Mesoporous high-surface-area activated carbon from biomass waste via microwave-assisted-H3PO4 activation for methylene blue dye adsorption: An optimized process, Diam. Relat. Mater. 128 (2022) 109288. https://doi.org/10.1016/J.DIAMOND.2022.109288.

[54] H. Xue, X. Wang, Q. Xu, F. Dhaouadi, L. Sellaoui, M.K. Seliem, A. Ben Lamine, H. Belmabrouk, A. Bajahzar, A. Bonilla-Petriciolet, Z. Li, Q. Li, Adsorption of methylene blue from aqueous solution on activated carbons and composite prepared from an agricultural waste biomass: A comparative study by experimental and advanced modeling analysis, Chem. Eng. J. 430 (2022) 132801. https://doi.org/10.1016/J.CEJ.2021.132801.

[55] F. Mbarki, T. Selmi, A. Kesraoui, M. Seffen, Low-cost activated carbon preparation from Corn stigmata fibers chemically activated using H3PO4, ZnCl2 and KOH: Study of methylene blue adsorption, stochastic isotherm and fractal kinetic, Ind. Crops Prod. 178 (2022) 114546. https://doi.org/10.1016/J.INDCROP.2022.114546.

[56] Y. Tan, X. Wang, F. Xiong, J. Ding, Y. Qing, Y. Wu, Preparation of lignin-based porous carbon as an efficient absorbent for the removal of methylene blue, Ind. Crops

Prod. 171 (2021) 113980. https://doi.org/10.1016/J.INDCROP.2021.113980.

[57] R. Zhu, J. Xia, H. Zhang, F. Kong, X. Hu, Y. Shen, W.H. Zhang, Synthesis of magnetic activated carbons from black liquor lignin and Fenton sludge in a one-step pyrolysis for methylene blue adsorption, J. Environ. Chem. Eng. 9 (2021) 106538. https://doi.org/10.1016/J.JECE.2021.106538.

[58] T.R. Brazil, M. Gonçalves, M.S.O. Junior, M.C. Rezende, Sustainable process to produce activated carbon from Kraft lignin impregnated with H3PO4 using microwave pyrolysis, Biomass and Bioenergy. 156 (2022) 106333. https://doi.org/10.1016/J.BIOMBIOE.2021.106333

[59] H.K. Yağmur, İ. Kaya, Synthesis and characterization of magnetic ZnCl2-activated carbon produced from coconut shell for the adsorption of methylene blue, J. Mol. Struct. 1232 (2021) 130071. https://doi.org/10.1016/J.MOLSTRUC.2021.130071.

[60] N.P. de Moraes, L.G.P. Marins, M.V. de Moura Yamanaka, R. Bacani, R. da Silva Rocha, L.A. Rodrigues, Efficient photodegradation of 4-chlorophenol under solar radiation using a new ZnO/ZnS/carbon xerogel composite as a photocatalyst, J. Photochem. Photobiol. A Chem. 418 (2021) 113377. https://doi.org/10.1016/j.jphotochem.2021.113377.

[61] A. Trenczek-Zajac, Thermally oxidized CdS as a photoactive material, New J. Chem. 43 (2019) 8892–8902. https://doi.org/10.1039/c9nj00484j.

[62] L.A. Rodrigues, L.J. Maschio, R.E. da Silva, M.L.C.P. da Silva, Adsorption of Cr(VI) from aqueous solution by hydrous zirconium oxide, J. Hazard. Mater. 173 (2010) 630–636. https://doi.org/10.1016/j.jhazmat.2009.08.131.

[63] S. Rattanapan, J. Srikram, P. Kongsune, Adsorption of Methyl Orange on Coffee grounds Activated Carbon, Energy Procedia. 138 (2017) 949–954. https://doi.org/10.1016/J.EGYPRO.2017.10.064.

[64] D. Ramutshatsha-Makhwedzha, A. Mavhungu, M.L. Moropeng, R. Mbaya, Activated carbon derived from waste orange and lemon peels for the adsorption of methyl orange and methylene blue dyes from wastewater, Heliyon. 8 (2022) e09930. https://doi.org/10.1016/J.HELIYON.2022.E09930.

[65] V. Yönten, N.K. Sanyürek, M.R. Kivanç, A thermodynamic and kinetic approach to adsorption of methyl orange from aqueous solution using a low cost activated carbon prepared from Vitis vinifera L., Surfaces and Interfaces. 20 (2020) 100529. https://doi.org/10.1016/J.SURFIN.2020.100529.

[66] B. Sun, Y. Yuan, H. Li, X. Li, C. Zhang, F. Guo, X. Liu, K. Wang, X.S. Zhao, Waste-cellulose-derived porous carbon adsorbents for methyl orange removal, Chem. Eng. J. 371 (2019) 55–63. https://doi.org/10.1016/J.CEJ.2019.04.031.

[67] B. Zhang, Y. Wu, L. Cha, Removal of methyl orange dye using activated biochar derived from pomelo peel wastes: performance, isotherm, and kinetic studies, Https://Doi.Org/10.1080/01932691.2018.1561298. 41 (2019) 125–136. https://doi.org/10.1080/01932691.2018.1561298.

[68] B.H. Hameed, L.H. Chia, S. Rengaraj, Adsorption of 4-chlorophenol onto activated carbon prepared from rattan sawdust, Desalination. 225 (2008) 185–198. https://doi.org/10.1016/j.desal.2007.04.095.

[69] V.M. Monsalvo, A.F. Mohedano, J.J. Rodriguez, Adsorption of 4-chlorophenol by inexpensive sewage sludge-based adsorbents, Chem. Eng. Res. Des. 90 (2012) 1807–1814. https://doi.org/10.1016/J.CHERD.2012.03.018.

[70] Z. Noorimotlagh, S. Shahriyar, R. Darvishi Cheshmeh Soltani, R. Tajik, Optimized adsorption of 4-chlorophenol onto activated carbon derived from milk vetch utilizing response surface methodology, New Pub Balaban. 57 (2015) 14213–14226. https://doi.org/10.1080/19443994.2015.1067830.

[71] T. Shen, P. Wang, L. Hu, Q. Hu, X. Wang, G. Zhang, Adsorption of 4-chlorophenol by wheat straw biochar and its regeneration with persulfate under microwave irradiation, J. Environ. Chem. Eng. 9 (2021) 105353. https://doi.org/10.1016/J.JECE.2021.105353.

[72] T.A. Kurniawan, W.H. Lo, M.E. Sillanpää, Treatment of Contaminated Water Laden with 4-Chlorophenol using Coconut Shell Waste-Based Activated Carbon Modified with Chemical Agents, Http://Dx.Doi.Org/10.1080/01496395.2010.512030. 46 (2011) 460–472. https://doi.org/10.1080/01496395.2010.512030.

[73] I. Enniya, L. Rghioui, A. Jourani, Adsorption of hexavalent chromium in aqueous solution on activated carbon prepared from apple peels, Sustain. Chem. Pharm. 7 (2018) 9–16. https://doi.org/10.1016/J.SCP.2017.11.003.

[74] Z.A. AL-Othman, R. Ali, M. Naushad, Hexavalent chromium removal from aqueous medium by activated carbon prepared from peanut shell: Adsorption kinetics, equilibrium and thermodynamic studies, Chem. Eng. J. 184 (2012) 238–247. https://doi.org/10.1016/J.CEJ.2012.01.048.

[75] M.K. Rai, G. Shahi, V. Meena, R. Meena, S. Chakraborty, R.S. Singh, B.N. Rai, Removal of hexavalent chromium Cr (VI) using activated carbon prepared from mango kernel activated with H3PO4, Resour. Technol. 2 (2016) S63–S70. https://doi.org/10.1016/J.REFFIT.2016.11.011.

[76] J. Zhao, L. Yu, H. Ma, F. Zhou, K. Yang, G. Wu, Corn stalk-based activated carbon synthesized by a novel activation method for high-performance adsorption of hexavalent chromium in aqueous solutions, J. Colloid Interface Sci. 578 (2020) 650–659. https://doi.org/10.1016/J.JCIS.2020.06.031.

Credit author statement

Nicolas Perciani de Moraes: Formal analysis; Investigation; Methodology; Software; Validation; Visualization; Writing; Writing - review & editing.

Flávio Henrique Covolam Boldrin: Formal analysis; Investigation; Methodology; Validation; Software; Visualization; Writing.

Tiago Moreira Bastos Campos: Formal analysis; Investigation; Methodology; Validation; Software; Visualization; Writing.

Gilmar Patrocinio Thim: Formal analysis; Funding acquisition; Investigation; Methodology; Validation; Software; Visualization; Writing.

Yu Lianqing: Formal analysis; Funding acquisition; Investigation; Methodology; Writing.

Marcos Roberto de Vasconcelos Lanza: Formal analysis; Funding acquisition; Investigation; Methodology; Writing.

Liana Alvares Rodrigues: Formal analysis; Funding acquisition; Investigation; Methodology; Project administration, Software; Supervision; Validation; Visualization; Writing; Writing - review & editing.

Declaration of interests

☒ The authors declare that they have no known competing financial interests or personal relationships that could have appeared to influence the work reported in this paper.

☐The authors declare the following financial interests/personal relationships which may be considered as potential competing interests:

.